Nuclear Instruments and Methods in Physics Research B 267 (2009) 3218–3222

Contents lists available at ScienceDirect

Nuclear Instruments and Methods in Physics Research B

journal homepage: www.elsevier.com/locate/nimb

Atomistic simulations of nanometric dislocation loops in bcc tungsten

J. Fikar *, R. Schäublin

Ecole Polytechnique Fédérale de Lausanne (EPFL), Centre de Recherche en Physique des Plasmas, Association Euratom-Confédération Suisse, CH 5332 Villigen PSI, Switzerland

ARTICLE INFO

Article history:
Available online 17 June 2009

PACS:
61.72.Lk
61.72.Nn
61.82.Bg

Keywords:
Radiation damage
bcc
Tungsten
Dislocation loops
Empirical potentials

ABSTRACT

Small dislocation loops formed from self-interstitial atoms (SIAs) are commonly found in irradiated metals. These defects significantly influence the mechanical properties of the materials. Atomistic simulations are used to describe nanometric circular dislocation loops with Burger's vectors $\frac{1}{2}a_0\langle 111\rangle$, $a_0\langle 100\rangle$ and $a_0\langle 110\rangle$ in bcc tungsten. Particular attention is paid to the habit plane of the $\frac{1}{2}a_0\langle 111\rangle$ loop. Two different embedded atom model (EAM) potentials are used. The energetics and geometry of the loops are studied as a function of their size.

1. Introduction

Due to its high melting point and good radiation resistance tungsten is a promising candidate for high temperature and irradiation applications e.g. divertor armor of the future fusion reactor. Interstitial loops are irradiation induced defects which are supposed to be the primary reason for irradiation hardening. The interstitial loops in tungsten are commonly observed after neutron or electron irradiation and after ion implantation [1–4]. $\frac{1}{2}a_0\langle 111\rangle$ Burger's vector was reported [1,2]. The same Burger's vector was also used in recent tungsten molecular dynamics simulations using one interatomic potential [5]. Here we also include other Burgers' vectors, which are possible in the bcc structure. The Burger's vector $a_0\langle 100\rangle$ is observed in Fe and Mo [6,7]. The $\frac{1}{2}a_0\langle 111\rangle$ loop with the habit plane $\{110\}$ is often suggested for Fe [8–11], while others suggest $\{111\}$ [12].

2. Computational method

Two EAM potentials for W are used in our atomistic simulations, performed in the NVT ensemble. There is the EAM potential by Ackland and Thetford (here denoted A) [13] and the recent EAM potential by Derlet, Nguyen-Manh and Dudarev (D) [14]. The lattice parameter a_0 is 3.1652 Å for both potentials. The main advantage of the recent D potential over the A potential is in the difference of formation energy of $\langle 110\rangle$ and $\langle 111\rangle$ interstitials, which is 0.7 eV and 0.3 eV for the potential A and D, respectively, while *ab initio* calculations predicts 0.2 eV [14]. Eyre and Bullough [15] proposed that in bcc metals interstitial loops nucleate as $\frac{1}{2}a_0\langle 110\rangle\{110\}$ with intrinsic stacking fault which then transform by shearing to $\frac{1}{2}a_0\langle 111\rangle\{110\}$ or at higher temperatures to $a_0\langle 100\rangle\{110\}$. As those loops grow, they are supposed to rotate to pure edge orientation *i.e.* $\frac{1}{2}a_0\langle 111\rangle\{111\}$ or $a_0\langle 100\rangle\{100\}$. Eyre and Bullough assumed that in all bcc the energetically most favorable interstitials are $\langle 110\rangle$, which is not the case of W. For that reason the loop $\frac{1}{2}a_0\langle 110\rangle\{110\}$ in W should be unstable, also because of the high energy of the intrinsic stacking fault. We consider Burgers' vectors $\frac{1}{2}a_0\langle 111\rangle$, $a_0\langle 100\rangle$ and $a_0\langle 110\rangle$. The $\frac{1}{2}a_0\langle 110\rangle$ loop is indeed extremely unstable using both potentials A or D and it does not transform via Eyre–Bullough mechanism to $\frac{1}{2}a_0\langle 111\rangle$ nor to $a_0\langle 100\rangle$. It is thus not considered here.

Circular interstitial dislocation loops are created by inserting discs of interstitials in a perfect cubic simulation box in such a way that no stacking fault is created. The number of inserted discs is summarized in Table 1 and the method itself is more detailed in [12].

To investigate the influence of the box size on the interstitial loop formation energy, two different cubic box sizes are used, a small one around 50^3a_0 and a large one close to 100^3a_0. As periodic boundary conditions are used, interaction between the loop and its periodic images also plays an important role. To determine the influence of this interaction on the formation energy, three different

* Corresponding author.
E-mail address: jan.fikar@psi.ch (J. Fikar).

0168-583X/$ - see front matter © 2009 Elsevier B.V. All rights reserved.
doi:10.1016/j.nimb.2009.06.075

box orientations are chosen. In this way the spatial arrangement of the loops is changed. For detailed description of the six used simulation boxes see Table 2.

The samples are relaxed using the conjugate gradient method. Perfect samples of the same geometry, but without any inserted disc, are also relaxed in the same manner. The formation energy of the dislocation loop is defined as the difference between the total energy after relaxation of the sample with the dislocation loop and that of the perfect sample scaled to the same number of atoms. The resulting formation energies for all simulation boxes in Table 2

Table 1
Number of inserted discs to create interstitial dislocation loops in bcc without stacking faults.

Burger's vector	Stacking sequence	No. of inserted discs
$\frac{1}{2}a_0\langle 111\rangle\{111\}$	ABC	3
$a_0\langle 100\rangle\{100\}$	AB	2
$a_0\langle 110\rangle\{110\}$	AB	2
$\frac{1}{2}a_0\langle 111\rangle\{110\}$	AB	1 displaced along $\langle 111\rangle$

Table 2
Detailed description of the simulation boxes. Number of atoms and orientation of the cube edges.

Orientation label	Small	Large	x	y	z
'100'	235,298	1,882,384	[100]	[010]	[001]
'110'	240,100	1,866,312	[110]	[001]	$[\bar{1}10]$
'111'	239,400	1,871,280	[111]	$[\bar{1}10]$	$[11\bar{2}]$

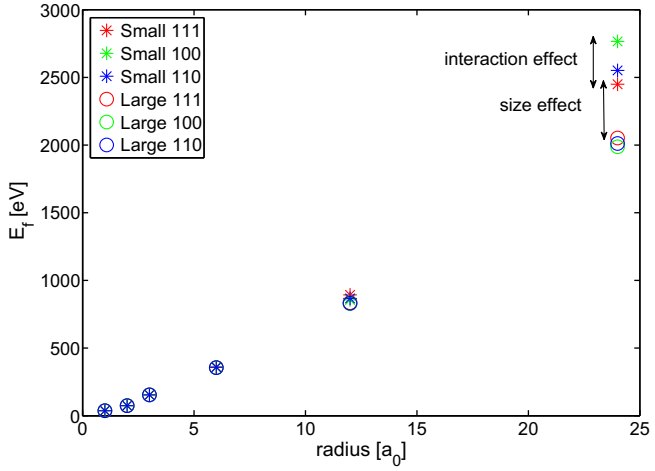

Fig. 1. Formation energy of $\frac{1}{2}a_0\langle 111\rangle\{111\}$ loop as a function of radius using the A potential and different simulation boxes. The effect of box size and loop interaction with its periodic images are highlighted by arrows.

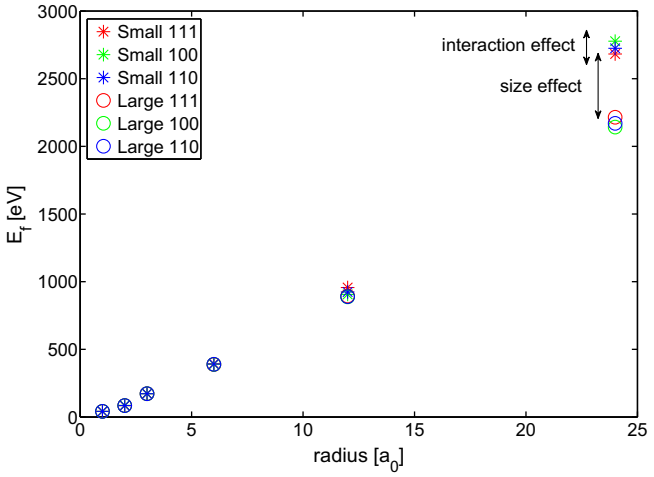

Fig. 2. Formation energy of $\frac{1}{2}a_0\langle 111\rangle\{111\}$ loop as a function of radius using the D potential and different simulation boxes. The effect of box size and loop interaction with its periodic images are highlighted by arrows.

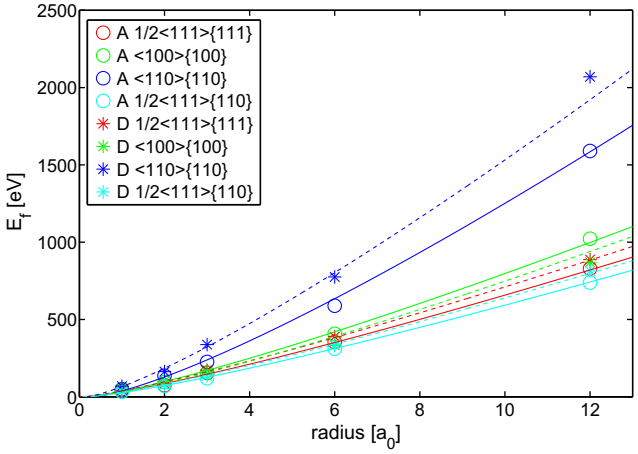

Fig. 3. Formation energy of interstitials loops using the large simulation box. The solid lines are the fit of Eq. (1) for the A potential, while dashed lines are for the D potential.

and $\frac{1}{2}a_0\langle 111\rangle\{111\}$ loops of radii between 1 and $24a_0$ are plotted in Figs. 1 and 2. It seems that a cubic box with a side at least $8\times$ larger than the loop diameter gives consistent formation energies within an error lower than 0.5 eV or 0.3%, while the box with a side $4\times$ larger than the loop diameter produces an error smaller than 6 eV or 1.5%. The optimal box orientations *i.e.* with lowest interaction of the loop with its periodic images are '111' for the $a_0\langle 100\rangle$ loop and '100' for the other loops. In the following we use the large

Table 3
Formation energies and dislocation core parameter for different dislocation loops and the potentials A and D.

Potential	Loop	$E_f[eV]$	Interstitials	$E_f[eV]$	Interstitials	$\rho[a_0]$
		$r = 2a_0$		$r = 6a_0$		
A	$\frac{1}{2}a_0\langle 111\rangle\{111\}$	74.3	19	355.3	199	0.14
	$a_0\langle 100\rangle\{100\}$	94.8	25	407.3	221	0.22
	$a_0\langle 110\rangle\{110\}$	136.0	31	589.3	315	0.54
	$\frac{1}{2}a_0\langle 111\rangle\{110\}$	70.1	17	310.7	159	0.23
D	$\frac{1}{2}a_0\langle 111\rangle\{111\}$	84.7	19	388.9	199	0.14
	$a_0\langle 100\rangle\{100\}$	100.9	25	332.8	221	0.22
	$a_0\langle 110\rangle\{110\}$	162.8	31	775.4	315	0.54
	$\frac{1}{2}a_0\langle 111\rangle\{110\}$	78.7	17	337.1	159	0.23